Comparative study of nitrogen doped multi walled carbon nanotubes grafted with carboxy methyl cellulose hybrid composite by inverse gas chromatography and its UV photo detectors application

Journal of Chromatography A 1670 (2022) 462997

Contents lists available at ScienceDirect

Journal of Chromatography A

journal homepage: www.elsevier.com/locate/chroma

Comparative study of nitrogen doped multi walled carbon nanotubes grafted with carboxy methyl cellulose hybrid composite by inverse gas chromatography and its UV photo detectors application

Basivi Praveen Kumar[a], Pasupuleti Visweswara Rao[b,c], Tayssir Hamieh[d,e,**], Chang Woo Kim[f,*]

[a] Pukyong National University Industry-University Cooperation Foundation, Pukyong National University, Busan 48513, Republic of Korea
[b] Center for International Collaboration and Research, Reva University, Rukmini Knowledge Park, Kattigenahalli Yelahanka, Bangalore, Karnataka 560064, India
[c] Department of Biochemistry, Faculty of Medicine and Health Sciences, Abdurrab University, Pekanbaru, Riau 28291, Indonesia
[d] Faculty of Science and Engineering, Maastricht University, P.O. Box 616, Maastricht, MD 6200, the Netherland
[e] Laboratory of Materials, Catalysis, Environment and Analytical Methods Laboratory (MCEMA), Faculty of Sciences, Lebanese University, Hadath, Lebanon
[f] Department of Nanotechnology Engineering, College of Engineering, Pukyong National University, Busan 48513, Republic of Korea

ARTICLE INFO

Article history:
Received 23 February 2022
Revised 22 March 2022
Accepted 24 March 2022
Available online 26 March 2022

Keywords:
Nitrogen doped MWCNTs
Hybrid composite
IGC
Specific free energy
London dispersive surface energy
Self-powered UV- photo detectors

ABSTRACT

In this present work, the synthesis of nitrogen doped multi walled carbon nanotubes (N-MWCNTs) grafted Sodium-carboxy methyl cellulose (Na-CMC) hybrid composite was carried out via thermal reduction process. The hybrid composites were thermodynamically characterized by inverse gas chromatography (IGC) and compared to Na-CMC particles. The results were obtained by using 14 different IGC methods and models. We proved that the free energy of adsorption of the different solvents on N-MWCNTs-Na-CMC surface was equal to the summation of both free enthalpies of the solvents separately adsorbed on N-MWCNT and on Na-CMC surfaces. The London dispersive surface free energy of different materials was calculated by using the various molecular models. The more precise results were obtained by Hamieh model based on the effect of the temperature on the surface area of organic molecules. It was proved that the dispersive component of the surface energy of N-MWCNTs-Na-CMC was equal to the geometric mean than that of N-MWCNTs and Na-CMC surfaces. Lewis Acid base properties of the various materials were determined by using the different models and methods. A stronger basic character was highlighted for the different solid surfaces with more accentuated acid base character for N-MWCNT solid. Furthermore, the potential usage of the hybrid nanocomposite was studied for the practical application of the self-powered UV photodetection. On the other hand, the N-MWCNTs-Na-CMC hybrid heterostructure N-MWCNTs-Na-CMC exhibited excellent photoresponse characteristics with a good stability and reproducibility under the UV illumination (λ=382 nm) at zero bias. The high photoresponse performances were mainly attributed to the improved conductivity and enhanced charge transfer resulting from the synergetic effect of N-MWCNTs-Na-CMC hybrid heterostructure. The detailed photoresponse properties of the N-MWCNTs-Na-CMC hybrid heterostructure was discussed in detail using energy band theory.

1. Introduction

The biodegradable packaging materials have recently got more attention due to environmental issues, because of their non-degradable and nonrenewable nature. In particular, the sodium carboxy methyl cellulose is one of the most important biodegradable polymers and exhibiting excellent properties [1–3]. The hydroxyl groups of cellulose can be reacted to give esters and ethers of different physical and chemical properties utilized for various potential applications [4,5]. Cellulose derivatives have significant roles used in the industry such as fibers, textiles, coatings, thermoplastics, food additives, and pharmaceutical materials [6–8]. In addition, the carbon nanotubes (CNTs) have recently emerged as wonder materials of the new century and are being considered for a whole host of applications ranging from large scale structures in automobiles to nanometer scale electronics [9,10]. The different carbon materials such as carbon nanotubes (CNTs), graphene oxide, porous metal organic framework containing the excellent ther-

* Corresponding author.
** Corresponding author at: Faculty of Science and Engineering, Maastricht University, P.O. Box 616, Maastricht, MD 6200, the Netherland.
E-mail addresses: t.hamieh@umaastrichtuniversity.nl (T. Hamieh), kimcw@pknu.ac.kr (C.W. Kim).

https://doi.org/10.1016/j.chroma.2022.462997
0021-9673/

mal conductivity, electrical conductivity, good mechanical strength for various potential applications [11–13], Particularly, the nitrogen doped multiwalled carbon nanotubes (N-MWCNT) having the larger surface area, excellent electrical conductivity, remarkable flexibility, and compatibility with increasing the structural and morphological properties [14,15]. Therefore, the N-MWCNT materials have been widely used for catalyst, supercapacitor, sensor, photodetectors [16], batteries, and electrocatalyst with excellent stability. The solid-state materials based on the MWCNTs fibrous electrode widely used for supercapacitor and catalytic applications in detail [17–21].

The inverse gas chromatography (IGC) is an efficient technique for describing these materials to explore their physicochemical properties [22–24]. The IGC technique is considered as a possible methodology due to its ability to ascertain their surface properties of crystalline solids and amorphous morphology in the form of fibers, powder, and films [25,26]. Based on the properties, the analytical gas chromatography techniques, IGC bears a unique spectacle of placing the material. Therefore, the column packing in presence of vapor used to accelerate the information on the surface of the substances [27]. The variety of properties such as entropy, enthalpy of adsorption, dispersive surface energy and solubility parameters were characterized by using IGC technique [27,28]. The information acquired from the IGC investigation supports to exploit the true potential of the materials and industrial applications in the various fields of research. In this present study, the determination of the net retention time of the organic solvents adsorbed on the solid surfaces by IGC technique allowed to obtain the free energy of adsorption on the chosen carbon nanotube materials, the dispersive parameters and specific factors of surface free energy by using the various molecular models [29–31]. The surface properties and the Lewis acid-base parameters were also calculated by using the various molecular surface areas, Hamieh model and the IGC methods based on the topological index, the deformation polarizability, the vapor pressure, the boiling point, the standard enthalpy of vaporization ΔH^0_{vap}, the enthalpy of vaporization as a function of the temperature $\Delta H^0_{vap}(T)$ and the enthalpy of formation ΔH^0_f of the injected solvents [32] to explore the nature of the surface of the nitrogen doped multiwalled carbon nanotubes (N-MWCNT) with carboxyl methyl cellulose (CMC) materials. Moreover, in recent days the demand for the ultraviolet (UV) photodetectors has gained a tremendous research attention owing to their importance in environmental monitoring, military, medicine and health care and civilian filed [16,33]. The exposure of UV radiation causes severe health hazardous to the organic life, that can damage the cell tissues, skin cancer, and eye problem etc. [34]. In particularly the self- powered UV photodetectors (PDs) has greatly been acknowledged in the research community, since it can operate without any external power supply [34,35]. Thus, these requirements can be achieved by making a hybrid heterostructured with a suitable bandgap and high electrical conductivity [36]. On the other side, the potential applicability of the CNTs and its derivative heterostructure have been widely explored in the UV photodetectors due their enhanced morphological, structural, physiochemical, optoelectrical properties and high surface to the volume ratio [36]. Accordingly, the hybrid heterojunction based on N-MWCNTs-Na-CMC would endows an efficient charge generation, separation and transportation, and minimizes the charge recombination probability that help to improve the device UV photodetection performances [34,36].

2. Thermodynamic methods and models

The net retention volume *Vn* of the different organic molecules adsorbed on the various N-MWCNTs surfaces was calculated from the IGC measurements by using the following relation [22–24]:

$$Vn = jD_c(t_R - t_0) \quad (1)$$

Where t_R is the retention time of the injected solvent, t_0 the zero-retention reference time, D_c the corrected flow rate and j the correction factor [37].

The standard free energy ΔG^0_a of adsorption of the probe (Eq. (3)):

$$\Delta G^0_a = -RT\ ln\ V_n + RT\ ln\left(\frac{P_0}{sm\ \pi_0}\right) \quad (2)$$

where R is the ideal gas constant, T the absolute temperature, m the mass of the solid, s its specific surface area, and P_0 and π_0 respectively the reference pressure and surface pressure depending on the reference state of adsorption [37]. We used here the Kemball and Rideal reference state [37] given at $T_0 = 0\ ^\circ C$ by $P_0 = 1.013 \times 10^5 Pa$ and $\pi_0 = 6.08 \times 10^{-5}\ N\ m^{-1}$.

The obtained free energy of adsorption ΔG^0_a can be divided to the dispersive ΔG^d_a and specific ΔG^{sp}_a contributions:

$$\Delta G^0_a = \Delta G^d_a + \Delta G^{sp}_a \quad (3)$$

The specific contributions of the free energy of adsorption of the probes was determined by using the different thermodynamic parameters, such as the vapor pressure P_0 [38,39], the boiling point *BP* [40], the deformation polarizability α_0 [41], the topological index χ_T [42], the standard enthalpy of vaporization ΔH^0_{vap} [32], the enthalpy of vaporization as a function of the temperature $\Delta H^0_{vap}(T)$ (new method), the standard enthalpy of formation ΔH^0_f (new method) of the injected solvents, Hamieh model [28] and six other methods based on the molecular models of the surface areas of organic molecules (for more details, see in Supporting Information).

These thermodynamic methods and models were used to determine the dispersive (London) and polar (specific) components of the free energy of adsorption. The specific free energy of adsorption ΔG^{sp}_a of used organic solvents was determined as a function of the temperature.

The following thermodynamic equation:

$$\Delta G^{sp}_a = \Delta H^{sp}_a - T\Delta S^{sp}_a \quad (4)$$

allowed to calculate the specific enthalpy ΔH^{sp}_a and entropy ΔS^{sp}_a of polar solvents adsorbed on the solid surfaces.

The determination of the specific enthalpy of adsorption $= \Delta H^{sp}_a$ allowed to calculate the acid K_A and base K_D constants of the different N-MWCNTs surfaces by using the following equation [38,39,43,44]:

$$\left(-\Delta H^{sp}_a\right) = K_A DN' + K_D AN' \quad (5)$$

where DN' and AN' are the normalized donor and acceptor numbers of electrons of the various probes [28–31].

On the other hand, the molecular models are based on the values of the surface area of the different n-alkanes and polar solvents, and Fowkes relation [45]:

$$-\Delta G^0_a = 2\mathcal{N}a\left(\gamma_l^d \gamma_s^d\right)^{1/2} + \left(-\Delta G^{sp}_a\right) \quad (6)$$

Where N is Avogadro's number, a is the surface area of one adsorbed molecule on the solid, and γ_l^d and γ_s^d are the dispersive components of the surface tension of the probe and of the solid respectively [45].

Relation 5 allowed to obtain γ_s^d of the solid and the specific contribution of adsorbed polar solvents. The surface area of organic molecules was obtained from the different following molecular models: Kiselev, Van der Waals, Redlich-Kwong, cylindric, geometric, spheric and Hamieh model based on the variation of a as a function of the temperature [27–29].

The calculation of γ_s^d of the different solids was also obtained by using Dorris and Gray relation [46] and Hamieh model combined to Dorris-Gray relation [47–49].

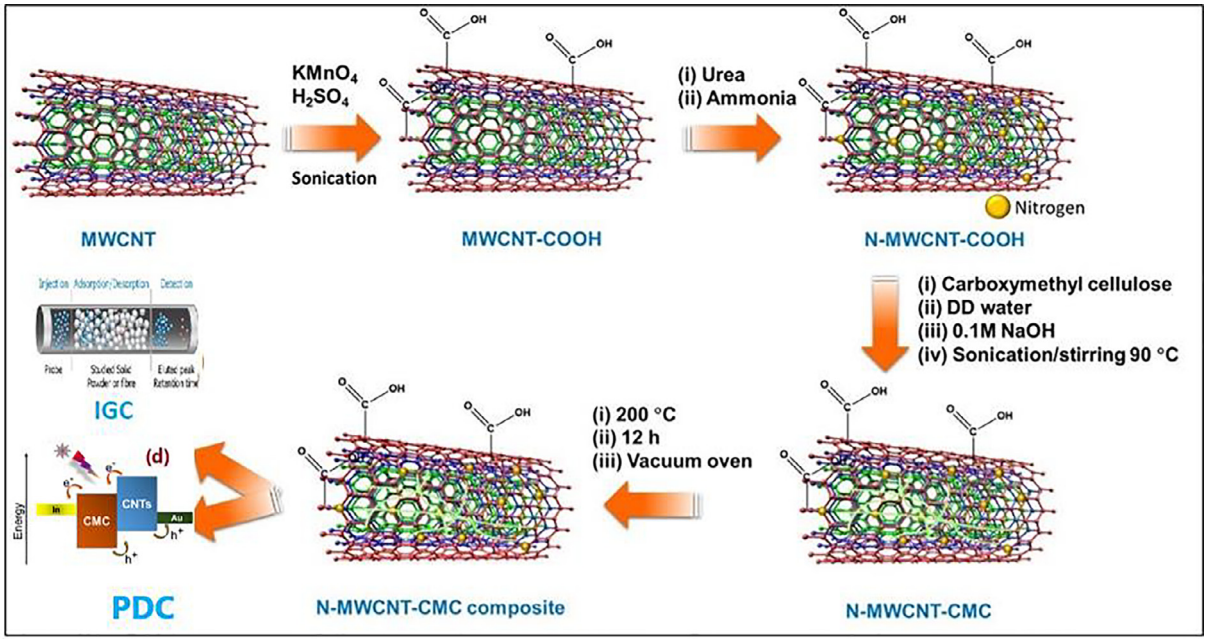

Fig. 1. Schematic illustration of N-MWCNT-Na-CMC composite.

3. Experimental

3.1. Materials

Analytical grade of Na-CMC ($\overline{M_n}$) of 90,000, N-MWCNTs, urea and ammonium hydroxide were purchased from Sigma-Aldrich Pvt., Ltd. (India) and used for column packing in this study. The solutes *n*-alkanes (C6–C10), acetone (AC), diethyl ether (DEE), tetrahydrofuran (THF), ethyl acetate (EA), chloroform (CH_3Cl) and dichloromethane (CH_2Cl_2) were analytical grade compounds purchased from Sigma-Aldrich Pvt., Ltd. (India). A stainless-steel column of 3 mm internal diameter and 50 cm length, received from (Sigma-Aldrich). The columns were perfectly washed with methanol and acetone solvent and then dried in the oven at 50°C.

3.2. Preparation of nitrogen doped multiwalled carbon nanotubes (N-MWCNTs)

The required amount of (3 g) of N-MWCNTs was taken into the round bottom flask and dissolved in the double distilled water, the reaction mixture was completely stirred for 300 ppm and 80°C. After that, the amount of 2.1 g of urea and 30 % ammonium hydroxide solution was added in the reaction mixture and continuously stirred for 12 h at same temperature. The reaction mixture washed by using ethanol and allowed to evaporate the solvent to get well dried reaction mixture of N-MWCNTs.

3.3. Preparation of N-MWCNTs -Na-CMC hybrid composite

The expected amount of 2.5 g of N-MWCNTs and 3 g of Na-CMC was taken into the round bottom flask and dissolved in the double distilled water, the reaction mixture was thoroughly stirred for 300 ppm spin and 80 °C continuously for 12 h. The calculated amount of 30 mL of 30% ammonium hydroxide solution was added in the reaction mixture and stirred for 12 h at 80°C. The reaction mixture washed by using methanol and ethanol solvents. Finally, the solvent allowed to evaporate via rotavapor and dried in the vacuum oven at 80°C for 12 h to complete the reaction product. The schematic diagram shown in Fig. 1

3.4. Column preparation

The collected reaction mixtures of hybrid composites were used for column preparation of 50 cm long, 3 mm internal diameter stain less tube cleaned with acetone and ethanol solvents. The column was filled by the solid particles (Na-CMC:1.400 g, N-MWCNTs: 1.400 g and N-MWCNTs-Na-CMC: 1.027g) using mechanical vibrator with continuous tapping system. After that the column packing at both ends plugged with silane-treated glass wool materials and conditioned with continuous purified helium flow overnight.

3.5. IGC experiments

Inverse gas chromatographic experimental measurements were carried out using a dual column AIMIL (model 5700, AIMIL Ltd, New Delhi) gas chromatograph (GC) coupled with flame ionization detector (FID). High purity (99.99%) helium was used for carrier gas at flow rate over the range 20 mL/min. The out let and in let pressure of the columns were measured at manometers. The measurements were carried out at constant oven temperature at intervals of 10 °C from 353.15 to 383.15 K. About 0.1 μL of each probe solute was injected using Hamilton microsyringe. The void volume V_0 of columns was obtained by measuring the dead retention time of methane t_0 for the used temperatures and served to determine the net retention volume of the probes. The corrected flow rate D_c and the correction James-Martin factor j [37] were used to determine the void volume, the total retention volume V_R and the net retention volume V_n of the probes by using the following relations: $V_0 = j\ D_c\ t_0$, $V_R = j\ D_c t_R$ and $V_n = V_R - V_0$. For each measurement, at least three repeated injections were made to obtain reproducible results used in the calculation of net retention volume V_n. The standard deviation was less than 1% in all measurements. The spectroscopic results were mentioned clearly in our previous published research article [53].

3.6. UV-photo detectors

Firstly, SiO_2 substrate was diced into the 1 × 1 cm samples and then clean organic solvents (ethanol, acetone and DI water) in order to remove the native oxides and particles. The optimized N-

MWCNTs-Na-CMC nanocomposite was spin coated on diced SiO_2 substrate with speed of 2000 rpm for 30 s and the sample was annealed at 50 °C for 40 min over the hotplate to allow the better adhesiveness. Thereafter, the Au metal contacts of 100 nm thickness and 1 mm diameter were deposited on the annealed samples through a shadow mask using e-beam evaporation, and indium was rubbed on the backside of the photodetector (PD) sample. In order to evaluate the photodetection performances of the N-MWCNTs-Na-CMC nanocomposite sample we have fabricated pristine CNT PD device for the comprehensive comparison.

The photoresponse characteristics of the as prepared samples were tested under the UV illumination (λ=382 nm) with a power density of 3.23 mW/cm^2. A mechanical chopper fan was positioned opposite to the sample to avoid the direct illumination. The corresponding, on/off photoresponse cycles were collected using the LabVIEW programmed PC externally connected to the Keithley-2400 and lock-in amplifier.

4. Results and discussion

4.1. IGC analysis

4.1.1. The gibbs free energy of adsorption

The IGC measurements of the net retention volume V_n of n-alkanes and polar probes led to the determination of the free energy $(-\Delta G_a)$ of adsorption on the Na-CMC, N-MWCNTs and N-MWCNTs-Na-CMC polymer particles (Table 1) at four different temperatures (353.15K–383.15K).

Results obtained showed larger free energy of adsorption $(-\Delta G_a)$ of all organic solvents on N-MWCNTs-Na-CMC compared to $(-\Delta G_a)$ of Na-CMC, N-MWCNTs.

It was proved that the sum of the free energies of adsorption relative to Na-CMC and N-MWCNTs (Table 2) was equal to the free energy of adsorption of the N-MWCNTs-Na-CMC polymer composite (Table 1):

$$-\Delta G_a)(N-MWCNTs-Na-CMC) = (-\Delta G_a)(N-MWCNTs)+(-\Delta G_a)(Na-CMC) \quad (7)$$

The above relation was proved valid for all organic molecules. This interesting result is conformed to the additivity principle of the free energy that is effectively considered as a variable of state. Indeed, for any state variable G, we can write thermodynamically in the case of a chemical compound *A-B*:

$$G\,(A-B) = G(A)+G(B) \quad (8)$$

We proved that the ratio [$(-\Delta G_a$(N-MWCNTs)) +($-\Delta G_a$(Na-CMC))]/[$(-\Delta G_a$(N-MWCNTs-Na-CMC))] (Table 3) is about 1.00 ± 0.05 showing the validity of the additivity principle of the free energy of adsorption.

The determination of $(-\Delta G_a)\,(T)$ of the various probes adsorbed on the three polymer materials as a function of materials led to evaluate the enthalpy and entropy of adsorption. On Table 4, we presented the values of the enthalpy $(-\Delta H_a\ in\ kJ\ mol^{-1})$ and entropy $(-\Delta S_a\ in\ J\,K^{-1}mol^{-1})$ of adsorption of the various polar solvents on N-MWCNTs (a), Na-CMC (b) and N-MWCNTs-Na-CMC (c). A strong enthalpy of interaction was showed (Table 4) in the case of the adsorption of organic molecules on the N-MWCNTs and greater than the enthalpy of Na-CMC and N-MWCNTs-Na-CMC.

The obtained results proved the following inequations:

$$1 < \frac{(-\Delta H_a)(N-MWCNTs)}{(-\Delta H_a)(N-MWCNTs-Na-CMC)} < 10 \quad (9)$$

$$5 < \frac{(-\Delta H_a)(N-MWCNTs)}{(-\Delta H_a)(Na-CMC)} < 50 \quad (10)$$

$$4 < \frac{(-\Delta H_a)(N-MWCNTs-Na-CMC)}{(-\Delta H_a)(Na-CMC)} < 6 \quad (11)$$

Table 1
Values of the free energy $(-\Delta G_a\ in\ kJ\ mol^{-1})$ of adsorption of the various polar solvents on N-MWCNT (a), Na-CMC (b) and N-MWCNT-Na-CMC (c) at various temperatures.

$-\Delta G_a$(N-MWCNT) (a)				
T(K)	353.15	363.15	373.15	383.15
C6	24.170	22.730	20.950	18.832
C7	29.367	27.028	24.235	20.903
C8	33.007	30.440	27.307	23.451
C9	34.828	32.342	29.416	25.841
C10	37.030	34.697	31.836	28.580
CH_2Cl_2	22.257	20.908	19.334	18.212
$CHCl_3$	21.468	20.144	18.885	17.704
Diethyl ether	21.733	20.103	18.500	17.495
THF	21.909	20.482	19.521	18.737
Ethyl acetate	24.170	22.122	20.953	19.788
Acetone	21.879	20.112	19.067	18.036
$-\Delta G_a$(Na-CMC) (b)				
T(K)	353.15	363.15	373.15	383.15
C6	9.818	9.717	9.617	9.516
C7	9.777	9.524	9.272	9.019
C8	10.323	10.090	9.856	9.622
C9	10.870	10.655	10.440	10.225
C10	11.193	10.921	10.650	10.378
CH_2Cl_2	9.770	9.550	9.220	8.870
$CHCl_3$	12.800	12.550	12.350	12.000
Diethyl ether	10.230	10.052	9.880	9.710
THF	10.350	10.000	9.800	9.630
Ethyl acetate	11.700	11.350	11.000	10.750
Acetone	11.000	10.680	10.340	9.980
$-\Delta G_a$ (N-MWCNT-Na-CMC) (c)				
T(K)	353.15	363.15	373.15	383.15
C6	30.850	29.924	28.903	27.416
C7	35.323	33.486	31.563	29.413
C8	38.318	36.421	34.361	32.168
C9	41.313	39.357	37.160	34.924
C10	44.668	42.871	40.669	38.079
CH_2Cl_2	32.300	30.220	28.645	27.112
$CHCl_3$	35.228	35.092	32.984	30.251
Diethyl ether	31.963	30.155	28.380	27.205
THF	33.726	32.236	30.608	28.254
Ethyl acetate	36.082	34.484	32.576	29.932
Acetone	33.406	32.208	30.264	28.427

Table 2
Values of $(-\Delta G_a(N{-}$MWCNT) + $(-\Delta G_a$(Na-CMC) of adsorption of the various polar solvents at various temperatures.

$(-\Delta G_a(N{-}$MWCNT) + $(-\Delta G_a$(Na-CMC)				
T(K)	353.15	363.15	373.15	383.15
C6	33.988	32.447	30.567	28.349
C7	39.143	36.552	33.507	29.922
C8	43.331	40.529	37.163	33.074
C9	45.697	42.996	39.856	36.065
C10	48.223	45.618	42.486	38.958
CH_2Cl_2	32.027	30.458	28.554	27.082
$CHCl_3$	34.268	32.694	31.235	29.704
Diethyl ether	31.963	30.155	28.380	27.205
THF	32.259	30.482	29.321	28.367
Ethyl acetate	35.870	33.472	31.953	30.538
Acetone	32.879	30.792	29.407	28.016

Proving that the enthalpy of adsorption $(-\Delta H_a)$ of the solvents on the three surfaces can be classified in increasing order as follows:

$$(Na-CMC) < (N-MWCNTs-Na-CMC) < (N-MWCNTs) \quad (12)$$

This result proved the important force of adsorption of the probes on N-MWCNT carbon nanotubes. On the other hand, the enthalpy of adsorption relative to polar molecules adsorbed on N-

Table 3
Values of the ration $[(-\Delta G_a(\text{N-MWCNT}))+(-\Delta G_a(\text{Na-CMC}))]/[(-\Delta G_a(\text{N-MWCNT-Na-CMC}))]$ at various temperatures.

$[(-\Delta G_a(N-\text{MWCNT}))+(-\Delta G_a(\text{Na-CMC}))]/[(-\Delta G_a(\text{N-MWCNT-Na-CMC}))]$					
T(K)	353.15	363.15	373.15	383.15	Average value
C6	1.10	1.08	1.06	1.03	1.10
C7	1.11	1.09	1.06	1.02	1.11
C8	1.13	1.11	1.08	1.03	1.13
C9	1.11	1.09	1.07	1.03	1.11
C10	1.08	1.06	1.04	1.02	1.08
CH_2Cl_2	0.99	1.01	1.00	1.00	0.99
$CHCl_3$	0.97	0.93	0.95	0.98	0.97
Diethyl ether	1.00	1.00	1.00	1.00	1.00
THF	0.96	0.95	0.96	1.00	0.96
Ethyl acetate	0.99	0.97	0.98	1.02	0.99
Acetone	0.98	0.96	0.97	0.99	0.98

Table 4
Values of the enthalpy ($-\Delta H_a$ *in* kJ mol^{-1}) and entropy ($-\Delta S_a$ *in* J K^{-1}mol^{-1}) of adsorption of the various polar solvents on N-MWCNT (a), Na-CMC (b) and N-MWCNT-Na-CMC (c).

N-MWCNT (a)		
Probes	$(-\Delta S_a)$	$(-\Delta H_a)$
C6	177.9	112.652
C7	281.8	129.138
C8	318.0	145.624
C9	298.9	140.634
C10	282.1	136.888
Dichloromethane	137.1	706.490
$CHCl_3$	125.5	657.590
Diethyl ether	143.2	721.670
THF	104.8	587.330
Ethyl acetate	143.1	744.540
Acetone	125.8	660.690
Na-CMC (b)		
Probes	$(-\Delta S_a)$	$(-\Delta H_a)$
C6	10.0	13.366
C7	25.3	18.694
C8	23.4	18.578
C9	21.5	18.461
C10	27.2	20.788
Dichloromethane	30.3	20.507
$CHCl_3$	26.0	21.997
Diethyl ether	17.3	16.344
THF	23.6	18.633
Ethyl acetate	32.0	22.981
Acetone	34.0	23.017
N-MWCNT-Na-CMC (c)		
Probes	$(-\Delta S_a)$	$(-\Delta H_a)$
C6	113.2	70.961
C7	196.5	104.810
C8	205.1	110.830
C9	213.7	116.850
C10	219.7	122.450
Dichloromethane	171.4	92.666
$CHCl_3$	170.4	96.117
Diethyl ether	160.5	88.511
THF	180.4	97.626
Ethyl acetate	203.6	108.220
Acetone	168.8	93.224

MWCNTs is more important than that of non-polar molecules, like n-alkanes (Table 4a). The results of the specific enthalpy of the adsorption of polar molecules on the different polymeric materials will be given in Section 4.1.3.

4.1.2. The London dispersive surface energy of materials

The dispersive component of the surface energy γ_s^d of the different solid substrates was determined by using the various molecular models such as Kiselev, Van der Waals, Redlich-Kwong, cylindric, geometric, spheric, Hamieh model (thermal model) [28], Dorris-Gray relation [46] and Hamieh-Dorris-Gray model [28,49]. The obtained results were given in Table 5. We proved for all used molecular models and Dorris-Gray method, the dispersive component of the surface energy of N-MWCNTs is the highest compared to other polymer surfaces.

Table 5
Values of the dispersive component of the surface energy γ_s^d (mJ/m^2) of N-MWCNT (a), Na-CMC (b) and N-MWCNT-Na-CMC (c) using the various models.

(N-MWCNT) (a)				
T(K)	353.15	363.15	373.15	383.15
Dorris-Gray	70.76	59.29	47.82	36.35
Gray-Hamieh model	108.58	88.10	67.62	47.15
Hamieh model	71.60	59.99	48.38	36.77
Spherical	157.96	136.01	114.05	92.09
Geometric	39.20	34.68	30.15	25.63
Redlich-Kwong	100.25	86.66	73.07	59.48
VDW	61.03	52.77	44.51	36.25
Cylindrical	52.03	45.65	39.26	32.87
Kiselev	53.63	46.85	40.08	33.30
Global average	79.44	67.77	56.09	44.42
γ_s^d (Na-CMC) (b)				
T(K)	353.15	363.15	373.15	383.15
Dorris-Gray	21.35	19.13	17.77	16.23
Gray-Hamieh model	36.44	33.05	29.11	25.23
Hamieh model	28.22	24.11	19.76	14.98
Spherical	60.20	49.62	43.66	38.17
Geometric	15.01	13.87	11.53	10.03
Redlich-Kwong	36.37	30.57	26.85	21.76
VDW	22.02	19.03	15.84	12.97
Cylindrical	20.34	18.27	16.19	14.12
Kiselev	18.90	16.37	13.84	11.32
Global average	29.38	26.01	22.64	19.27
γ_s^d (N-MWCNT-Na-CMC) (c)				
T(K)	353.15	363.15	373.15	383.15
Dorris-Gray	39.55	34.74	29.93	25.12
Gray-Hamieh model	60.77	51.49	42.20	32.92
Hamieh model	44.39	37.30	30.20	23.11
Spherical	97.47	84.25	71.03	57.80
Geometric	24.49	21.74	18.99	16.24
Redlich-Kwong	61.29	53.26	45.22	37.18
VDW	37.34	32.45	27.56	22.67
Cylindrical	32.37	28.50	24.63	20.75
Kiselev	33.37	29.25	25.13	21.01
Global average	47.90	41.45	35.00	28.54

Table 5 showed the following classification whatever the applied molecular model:

$$\gamma_s^d(N-MWCNTs) > \gamma_s^d(N-MWCNTs-Na-CMC) > \gamma_s^d(Na-CMC) \quad (13)$$

The result given by relation (7) showing the additivity of the free energy of adsorption, suggested to us to calculate the geometric mean of $\gamma_s^d(A)$ (of polymer Na-CMC) and $\gamma_s^d(A)$ (of polymer N-MWCNTs) and to show that this geometric mean is none other than the dispersive component of the surface energy $\gamma_s^d(A-B)$ of N-MWCNTs-Na-CMC polymer composite. This interesting and precious result can be represented by the following relation with an excellent accuracy (less than 3%):

$$\gamma_s^d(A-B) = \sqrt{\gamma_s^d(A)}\,\sqrt{\gamma_s^d(B)} \quad (14)$$

On Fig. 2 we gave the comparison between the various London dispersive surface energy and showed the validity of relation (14) by choosing Hamieh model for example.

The γ_s^d values are decreasing with increasing of the temperature for all polymer composites. The highest value of $\gamma_s^d(N-MWCNTs)$ relatively to $(N-MWCNTs-Na-CMC)$ can be explained in terms of chemical or physical polymer structure of

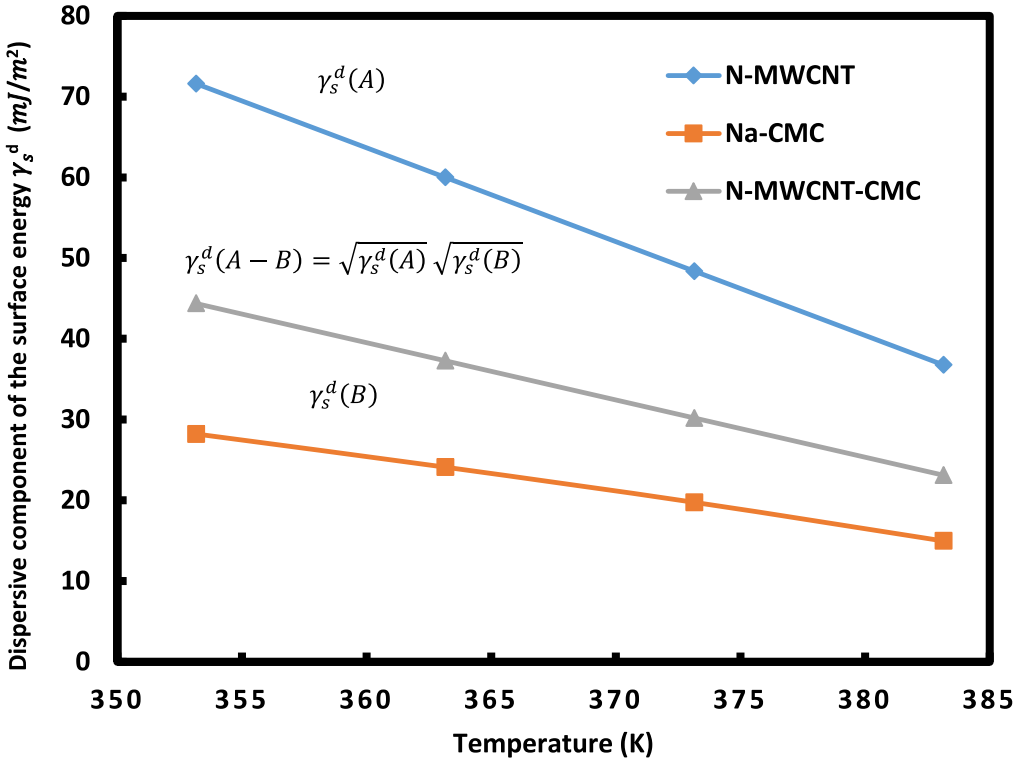

Fig. 2. Variations of the London dispersive surface energy γ_s^d (mJ/m^2) of MWCNT (A), CMC (B) and MWCNT-Na-CMC (A-B) as a function of the temperature T (K) using Hamieh model.

the material. The two above samples contain N-MWCNTs whereas, Na – CMC polymer contains some chemical and hydrogen bonding interactions with the probe solutes. The presence of functional groups rings active surface sites, in other words, physical interactions are interactive blending of the -NH_2 group. This may also lead to increase in the London dispersive surface free energy of the N- MWCNTs-Na-CMC polymer composite. The intramolecular hydrogen bonding and N-MWCNTs repulsion occurred between probes and polymeric Na-CMC materials. The γ_s^d values are indicating that the surface of the solid material as getting structured changes that allowed for the penetration of the probe molecules. The temperature gradient of γ_s^d is negative (Table 6) which may be attributed to the increase in the distance of accession between the N-MWCNTs and polymeric molecules with increase of temperature.

The London dispersive energy is inversely proportional to the sixth power of the distance of separation between the molecules. Therefore, with the increase of temperature, the distance of dissolution between molecules also increases and the dispersive energy decreases [50,51].

On Table 6, we gave the different equations $\gamma_s^d(T)$ of N-MWCNTs (a), Na-CMC (b) and N-MWCNTs-Na-CMC (c) for various molecular models of n-alkanes as a function of the temperature. We also determined the values of the dispersive surface entropy ε_s^d, the extrapolated values $\gamma_s^d(T=0K)$ for the different molecular models (Table 6). The more precise model giving the more accurate values of γ_s^d is that given by Hamieh model taking into account the thermal effect on the surface areas of the various used n-alkanes [28,52]. Expressions 11–13 gave the variations of γ_s^d as a function of the temperature for the three studied polymeric materials:

$$\gamma_s^d(T)\ (N-MWCNTs) = -1.16\,T + 481.68 \quad (15)$$

$$\gamma_s^d(T)\ (Na-CMC) = -0.44\,T + 184.01 \quad (16)$$

$$\gamma_s^d(T)\ (N-MWCNTs-CMC) = -0.71\,T + 294.95 \quad (17)$$

4.1.3. The specific thermodynamic variables and Lewis's acid-base parameters

The values of the specific free energy $(-\Delta G_a^{sp})$ of adsorption of the probes on the various polymeric materials were obtained from Eq. (3) by using the different IGC methods based on the following parameters, such as P_0 [38,39], BP [40], α_0 [41], ΔH_{vap}^0 [32], χ_T [42], $\Delta H_{vap}^0(T)$, ΔH_f^0 and seven other molecular models depending of the surface areas of organic molecules. The values of $(-\Delta G_a^{sp})$ of different polar solvents adsorbed on the various polymeric materials were given on Tables S.I.1. and S.I.2. as a function of the temperature by using the different molecular models and IGC methods. The results proved an important difference between the behavior of the different materials. The highest specific interactions were obtained for N-MWCNTs followed by the N-MWCNTs-Na-CMC polymer composite and then Na-CMC polymer whatever the used model or method. A strong tendency of amphoteric character was observed for N-MWCNTs with highest basic property. This acid base character decreases from N-MWCNTs to N-MWCNTs-Na-CMC and Na-CMC. To confirm this property, we estimated the specific enthalpy of adsorption ΔH_a^{sp} and specific entropy of adsorption ΔS_a^{sp} using Eq. (4). The representation of $(-\Delta G_a^{sp})$ (T) as a function of the temperature (Fig. 3), for the various materials, exhibited a linear variation with a good linear regression coefficient approaching the unit for all IGC methods and models.

$(-\Delta G_a^{sp})$ (T) gave the values of $(-\Delta S_a^{sp})$ and $(-\Delta H_a^{sp})$ respectively from the slope and intercept of the straight line $(-\Delta G_a^{sp})$ (T). Furthermore, the $(-\Delta H_a^{sp})$ values along with Lewis's acid-base parameters have been used in Eq. (5) to evaluate their Lewis acid-base parameters. Tables 7 and 8 gave the values of

Table 6
Equations $\gamma_s^d(T)$ of N-MWCNT (a), Na-CMC (b) and N-MWCNT-Na-CMC (c) for various molecular models of n-alkanes, and values of the dispersive surface entropy ε_s^d and the extrapolated values $\gamma_s^d(T=0K)$ by using the different molecular models.

N-MWCNT (a)

Molecular model	γ_s^d (in mJ/m^2)	$\frac{d\gamma_s^d}{dT}$ (in mJ m^{-2} K^{-1})	$\gamma_s^d(T=0K)$ (in mJ/m^2)
Dorris-Gray	$\gamma_s^d(T)$ = -1.15 T + 475.86	-1.15	475.86
Gray-Hamieh model	$\gamma_s^d(T)$ = -2.05 T + 831.76	-2.05	831.76
Hamieh model	$\gamma_s^d(T)$ = -1.16 T + 481.68	-1.16	481.68
Spherical	$\gamma_s^d(T)$ = -2.20 T + 933.41	-2.20	933.41
Geometric	$\gamma_s^d(T)$ = -0.45 T + 198.93	-0.45	198.93
Redlich-Kwong	$\gamma_s^d(T)$ = -1.36 T + 580.18	-1.36	580.18
VDW	$\gamma_s^d(T)$ = -0.83 T + 352.77	-0.83	352.77
Cylindrical	$\gamma_s^d(T)$ = -0.64 T + 277.59	-0.64	277.59
Kiselev	$\gamma_s^d(T)$ = -0.68 T + 292.85	-0.68	292.85
Global average	$\gamma_s^d(T)$ = -1.17 T + 491.67	-1.17	491.67

Na-CMC (b)

Molecular model	γ_s^d (in mJ/m^2)	$\frac{d\gamma_s^d}{dT}$ (in mJ m^{-2} K^{-1})	$\gamma_s^d(T=0K)$ (in mJ/m^2)
Dorris-Gray	$\gamma_s^d(T)$ = -0.17 T + 80.19	-0.17	80.19
Gray-Hamieh model	$\gamma_s^d(T)$ = -0.38 T + 169.25	-0.38	169.25
Hamieh model	$\gamma_s^d(T)$ = -0.44 T + 184.01	-0.44	184.01
Spherical	$\gamma_s^d(T)$ = -0.72 T + 313.13	-0.72	313.13
Geometric	$\gamma_s^d(T)$ = -0.17 T + 76.226	-0.17	76.226
Redlich-Kwong	$\gamma_s^d(T)$ = -0.48 T + 203.93	-0.48	203.93
VDW	$\gamma_s^d(T)$ = -0.30 T + 129.10	-0.3	129.1
Cylindrical	$\gamma_s^d(T)$ = -0.21 T + 93.51	-0.21	93.51
Kiselev	$\gamma_s^d(T)$ = -0.25 T + 108.14	-0.25	108.14
Global average	$\gamma_s^d(T)$ = -0.34 T + 148.29	-0.34	148.29

N-MWCNT-Na-CMC (c)

Molecular model	γ_s^d (in mJ/m^2)	$\frac{d\gamma_s^d}{dT}$ (in mJ m^{-2} K^{-1})	$\gamma_s^d(T=0K)$ (in mJ/m^2)
Dorris-Gray	$\gamma_s^d(T)$ = -0.48 T + 209.38	-0.48	209.38
Gray-Hamieh model	$\gamma_s^d(T)$ = -0.93 T + 388.67	-0.93	388.67
Hamieh model	$\gamma_s^d(T)$ = -0.71 T + 294.95	-0.71	294.95
Spherical	$\gamma_s^d(T)$ = -1.32 T + 564.48	-1.321	564.48
Geometric	$\gamma_s^d(T)$= -0.28 T + 121.57	-0.28	121.57
Redlich-Kwong	$\gamma_s^d(T)$ = -0.80 T + 345.12	-0.80	345.12
VDW	$\gamma_s^d(T)$ = -0.49 T + 209.92	-0.49	209.92
Cylindrical	$\gamma_s^d(T)$ = -0.39 T + 169.11	-0.39	169.11
Kiselev	$\gamma_s^d(T)$ = -0.415 T + 178.94	-0.419	178.94
Global average	$\gamma_s^d(T)$ = -0.65 T + 275.79	-0.65	275.79

$(-\Delta H_a^{sp})$ and $(-\Delta S_a^{sp})$ of the various polar molecules adsorbed respectively on N-MWCNTs and N-MWCNTs-Na-CMC surfaces for the different IGC methods and models.

Knowing the normalized acceptor AN' and donor DN' numbers of the polar solvents [27,29,48], we drew on Figs. 4 and 5 the variations of $(-\Delta H_a^{sp})/AN'$ and $(-\Delta S_a^{sp})/AN'$ as a function of DN'/AN' of the different polar molecules for N- MWCNTs and N-MWCNTs-Na-CMC polymer composite samples.

The values of acidic K_A and basic K_D constants of the different materials were obtained by using Eq. (5) from the slope and intercept of the liner plots respectively in all 14 methods and models. Whereas, the entropic acid ω_A and base ω_D constants were obtained from Eq. (18):

$$\left(-\Delta S_a^{sp}\right) = \omega_A DN' + \omega_D AN' \tag{18}$$

The values of enthalpic and entropic acid base constants were given on Table 9 for N-MWCNT, Na-CMC and N-MWCNTs-Na-CMC polymeric materials as well as their acid base ratios by using the above 14 molecular models and methods.

The values presented on Table 9 clearly showed highest K_A, K_D, ω_A and ω_D acid base constants for N- doped MWCNTs respectively followed by N-MWCNTs -Na-CMC and Na-CMC polymers. Results of Table 9 showed a strong basic character of the various polymeric materials. We obtained the following average values of the different acid base parameters of the three surfaces obtained by the different models: For N-MWCNTs, K_A = 0.82, K_D = 1.79, $\omega_A = 2.1 \times 10^{-3}$ and $\omega_D = 5 \times 10^{-3}$; for N-MWCNTs-Na-CMC: K_A = 0.17, K_A = 0.82, $\omega_A = 4.8 \times 10^{-4}$ and $\omega_D = 1.9 \times 10^{-3}$; and for Na-CMC: K_A = 0.05, K_D = 0.47, $\omega_A = 1.17 \times 10^{-4}$ and $\omega_D = 8.3 \times 10^{-4}$. These average acid base values are very close to that obtained by using Hamieh model that gave for N-MWCNTs, K_A = 0.89, K_D = 1.85, $\omega_A = 2.1 \times 10^{-3}$ and $\omega_D = 5 \times 10^{-3}$; for N-MWCNTs-Na-CMC: K_A = 0.27, K_A = 0.57, $\omega_A = 8.3 \times 10^{-4}$ and $\omega_D = 1.2 \times 10^{-3}$; and for Na-CMC: K_A = 0.09, K_D = 0.17, $\omega_A = 1.25 \times 10^{-4}$ and $\omega_D = 8.5 \times 10^{-4}$. The superiority of Hamieh model results from taking into account the thermal effect on the surface area [28] of the solvents that led to more accurate values of acid base parameters.

For the 14 used models and methods, one can classify the three studied materials in decreasing order of their acidic and basic constants:

$$K_A(N-MWCNTs) > K_A(N-MWCNTs-Na-CMC) > K_A(Na-CMC) \tag{19}$$

$$K_D(N-MWCNTs) > K_D(N-MWCNTs-Na-CMC) > K_D(Na-CMC) \tag{20}$$

$$w_A(N-MWCNTs) > w_A(N-MWCNTs-Na-CMC) > w_A(Na-CMC) \tag{21}$$

$$w_D(N-MWCNTs) > w_D(N-MWCNTs-Na-CMC) > w_D(Na-CMC) \tag{22}$$

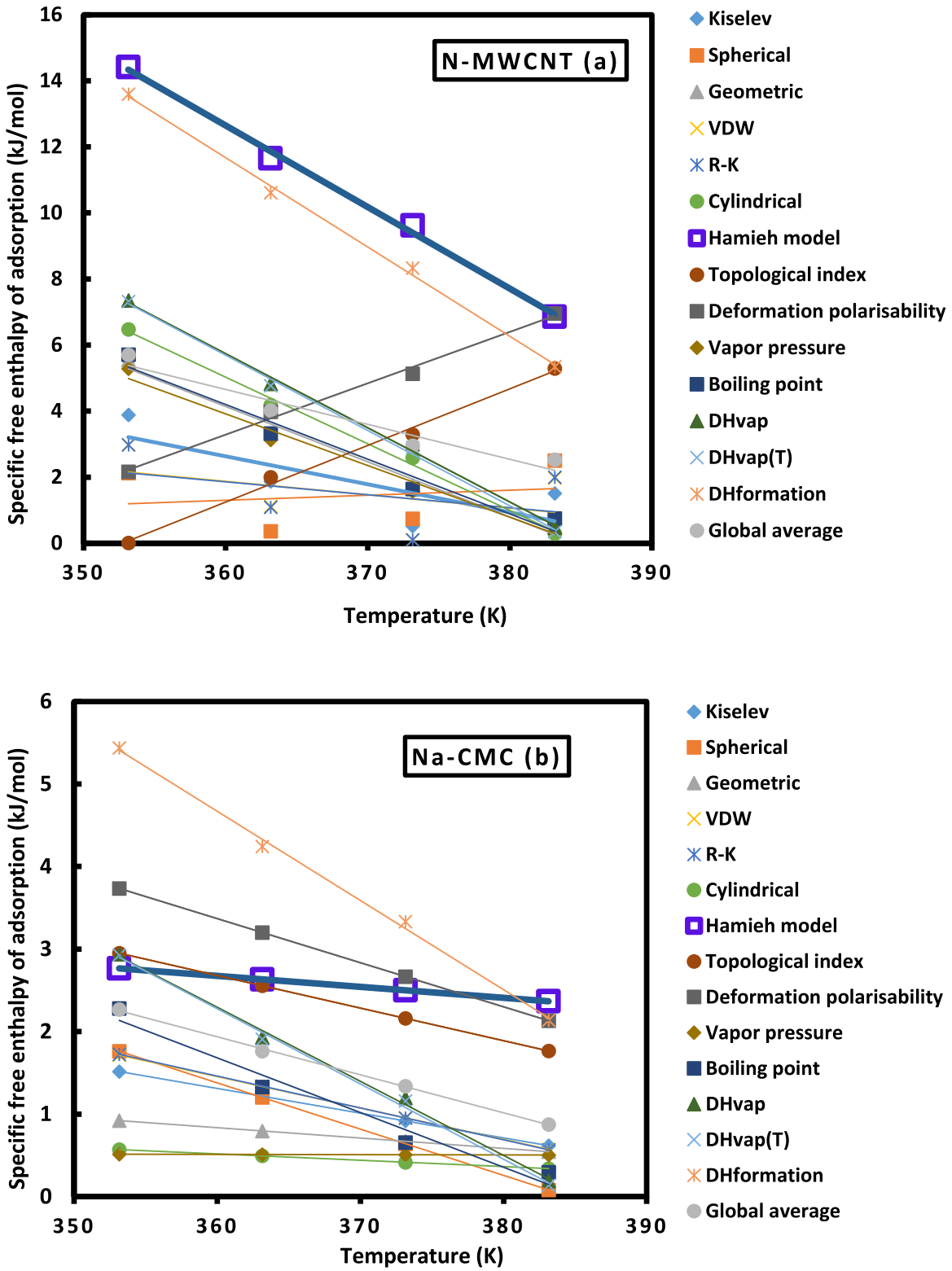

Fig. 3. Variations of $\Delta G_a^{sp}(T)$ as a function of the temperature of acetone adsorbed on N-MWCNT (a), Na-CMC (b) and N-MWCNT-Na-CMC (c) surfaces by using the different IGC models and methods.

We observed that the same order was obtained by Eq. (13) for the London dispersive surface energy of the different materials. This implied that the material exhibiting higher acid base constants has also higher dispersive surface energy. The obtained results suggest that the N- MWCNTs contain more basic sites than the N-MWCNTs-Na-CMC polymer composite and Na-CMC surfaces and can interact strongly in the Lewis acidic media. The overall character of the three surfaces is basic in nature. However, an amphoteric character was observed in the N- MWCNTs showing that this material can also interact in the Lewis basic media.

On the other hand, we proved by calculation that the geometric mean of any acid base parameter X of Na-CMC and N-MWCNTs polymers was equal to that of N-MWCNTs-Na-CMC polymer composite. This can be expressed by Eq. (23) with a good accuracy (less

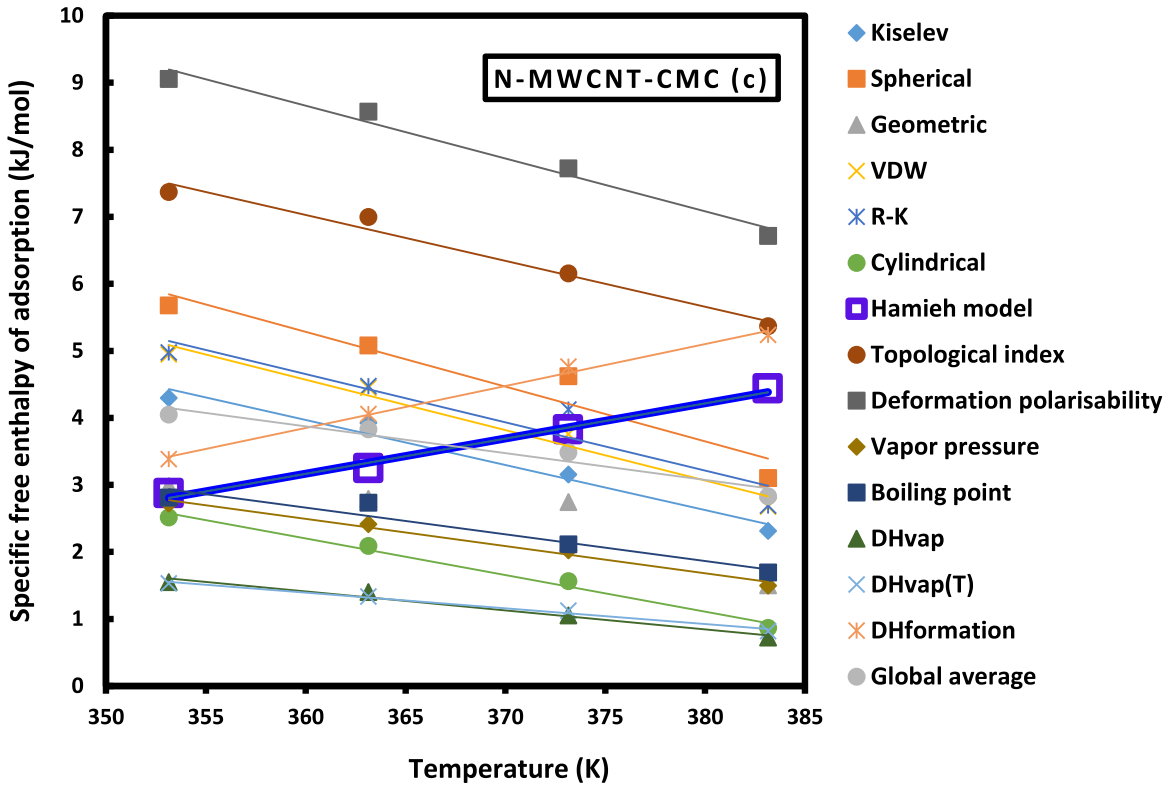

Fig. 3. Continued

Table 7
Values of the specific enthalpy ($-\Delta H_a^{sp}$ *in kJ* mol^{-1}) of the various polar solvents adsorbed on N-MWCNT (a) and N-MWCNT-Na-CMC (b) surfaces by using the various molecular models, Hamieh model, topological index, deformation polarizability, vapor pressure, boiling point, standard enthalpy of vaporization and enthalpy of formation methods compared to global average.

N-MWCNT (a) Probes	CH_2Cl_2	$CHCl_3$	Diethyl ether	THF	Ethyl acetate	Acetone
Kiselev	97.878	65.097	62.017	80.749	61.171	65.654
Spherical	85.546	52.362	65.488	66.714	50.731	54.739
Geometric	79.38	10.207	76.358	79.508	57.404	75.032
VDW	88.103	40.571	66.542	65.542	54.976	59.671
Redlich-Kwong	87.531	40.347	66.04	65.431	55.005	59.641
Cylindrical	74.258	14.541	78.682	87.957	62.086	77.58
Hamieh model	113.15	14.418	70.452	83.548	68.104	101.59
Topological index	67.017	32.542	70.898	65.63	59.019	60.46
Deformation polarizability	107.17	49.591	65.325	55.019	52.133	52.687
Vapor pressure	80.982	52.179	56.953	69.746	51.327	72.861
Boiling point *BP*	90.621	62.659	67.938	75.803	67.283	79.837
ΔH_{vap}^0	102.83	62.683	74.571	80.397	72.956	86.568
$\Delta H_{vap}^0(T)$	99.277	58.756	69.494	76.769	64.227	87.745
Enthalpy of formation ΔH_f^0	72.810	35.996	119.950	87.160	141.130	109.020
Average values	89.040	42.282	72.193	74.284	65.539	74.506

N-MWCNT-CMC (b) Probes	CH_2Cl_2	$CHCl_3$	Diethyl ether	THF	Ethyl acetate	Acetone
Kiselev	21.639	31.514	16.631	8.2611	20.736	28.181
Spherical	29.596	27.042	14.433	19.01	29.184	34.725
Geometric	34.911	16.185	7.3503	21.526	23.893	19.046
VDW	31.786	28.7	15.466	20.161	26.069	31.589
Redlich-Kwong	27.467	23.499	13.7	19.713	25.594	30.55
Cylindrical	40.059	31.179	6.1969	24.075	21.303	21.859
Hamieh model	15.037	22.114	39.103	23.738	17.984	15.756
Topological index	44.559	45.677	11.712	20.28	23.053	31.656
Deformation polarizability	15.124	33.517	15.919	29.346	28.065	37
Vapor pressure	28.529	27.275	9.5197	14.721	23.813	17.102
Boiling point *BP*	28.155	23.926	13.223	12.621	16.101	17.001
ΔH_{vap}^0	17.719	22.776	9.109	9.9233	11.981	11.633
$\Delta H_{vap}^0(T)$	20.98	21.785	13.488	13.965	19.257	9.8408
Enthalpy of formation ΔH_f^0	42.038	44.238	7.1912	4.5676	19.377	18.705
Average values	28.400	28.531	13.789	17.279	21.886	23.189

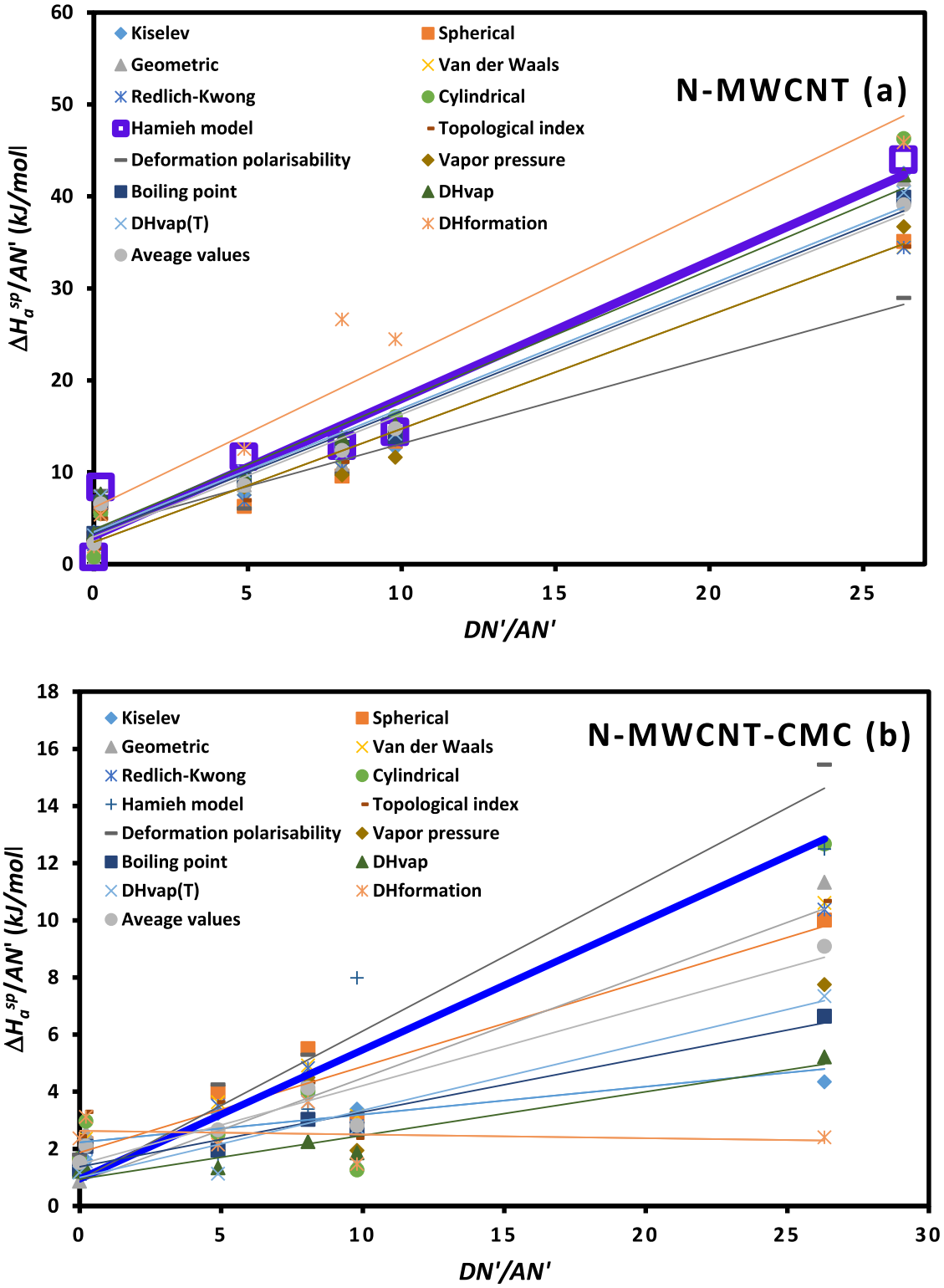

Fig. 4. Variations of $(\frac{-\Delta H_a^{sp}}{AN'})$ as a function of $(\frac{DN'}{AN'})$ of different polar molecules adsorbed on N-MWCNT (a) and N-MWCNT-Na-CMC (b) surfaces for different molecular models and IGC methods.

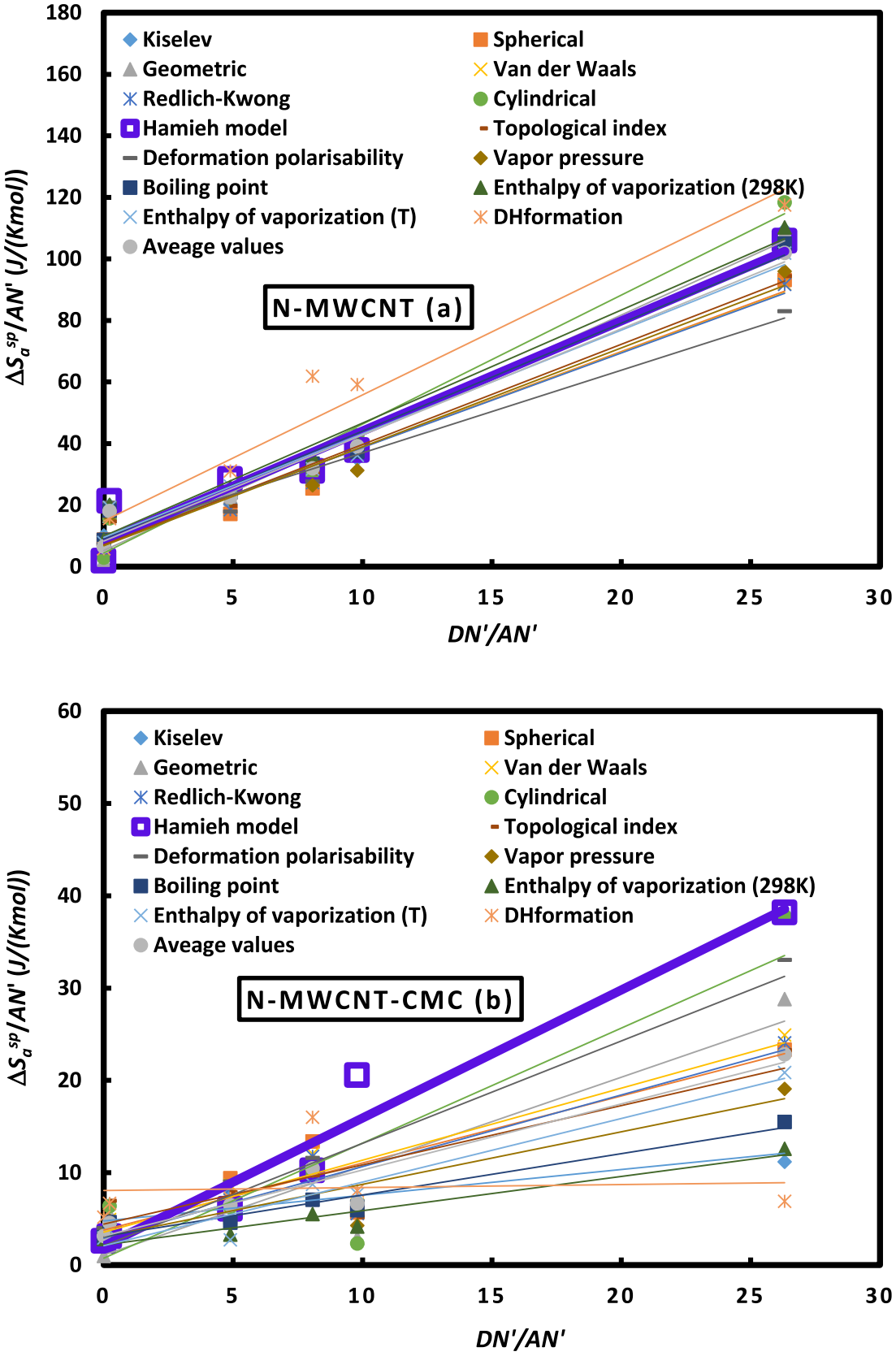

Fig. 5. Variations of $(\frac{-\Delta S_a^{sp}}{AN'})$ as a function of $(\frac{DN'}{AN'})$ of different polar molecules adsorbed on N-MWCNT (a) and N-MWCNT-Na-CMC (b) surfaces for different molecular models and IGC methods.

Table 8
Values of the specific entropy ($-\Delta S_a^{sp} in\ J\ K^{-1} mol^{-1}$) of the various polar solvents adsorbed on N-MWCNT (a) and N-MWCNT-Na-CMC (b) surfaces by using the various molecular models, Hamieh model, topological index, deformation polarizability, vapor pressure, boiling point, standard enthalpy of vaporization and enthalpy of formation methods compared to global average.

N-MWCNT (a) Probes	CH_2Cl_2	$CHCl_3$	Diethyl ether	THF	Ethyl acetate	Acetone
Kiselev	268.7	188.1	171.4	207.9	157.8	175.1
Spherical	241.6	163.2	181.7	177	134.5	149.2
Geometric	222.4	37.5	203.8	206.6	152.6	196.9
VDW	245.8	127	182.7	174.5	144.5	160.7
Redlich-Kwong	244.4	126.6	181.5	174.2	144.6	160.7
Cylindrical	211.8	53.9	209.04	224.9	161.4	201.5
Hamieh model	287.8	33.8	185	201.2	164.5	247.1
Topological index	198.3	101.5	189.9	179.3	160.6	171.4
Deformation polarizability	280	136.2	178.4	157.7	146.5	155.5
Vapor pressure	219.4	136.2	152.9	182.2	140	191.5
Boiling point *BP*	245.4	162.4	182.7	199.4	177	210.1
ΔH_{vap}^0	271	162.9	197.2	209.4	188.9	224.5
$\Delta H_{vap}^0(T)$	260.1	145.5	176.9	193.5	168.4	227.9
Enthalpy of formation ΔH_f^0	210.1	108.5	289.8	223.2	328	270.4
Global average	268.7	188.1	171.4	207.9	157.8	175.1

N-MWCNT-Na-CMC (b) Probes	CH_2Cl_2	$CHCl_3$	Diethyl ether	THF	Ethyl acetate	Acetone
Kiselev	42.2	66.1	34.2	21.2	51.8	67.3
Spherical	58.9	44.8	27.8	44.3	70.8	81.8
Geometric	74.4	18	14.3	54.7	56.4	44.9
VDW	66.4	51.9	32	47.3	63.7	75.1
Redlich-Kwong	54.5	36.8	27.2	45.7	62.3	71.9
Cylindrical	86.2	58.5	11.3	71.8	52.7	54.6
Hamieh model	41.7	48.2	100.6	72.5	54.2	52.6
Topological index	93.7	98.3	25.4	44.2	51.5	68.4
Deformation polarizability	35.7	74.6	33.9	62.8	61.4	78.7
Vapor pressure	64.5	63.7	20.9	36.2	54.1	40.6
Boiling point *BP*	62.6	55.8	29	29.4	37.4	39.8
ΔH_{vap}^0	40.5	52.5	20.4	23.9	29.1	28.4
$\Delta H_{vap}^0(T)$	50.3	54.5	37.6	39.6	46.2	23.5
Enthalpy of formation ΔH_f^0	89.9	96.7	39.4	13.1	84.8	62.7
Global average	61.5	58.6	32.4	43.3	55.45714	56.45

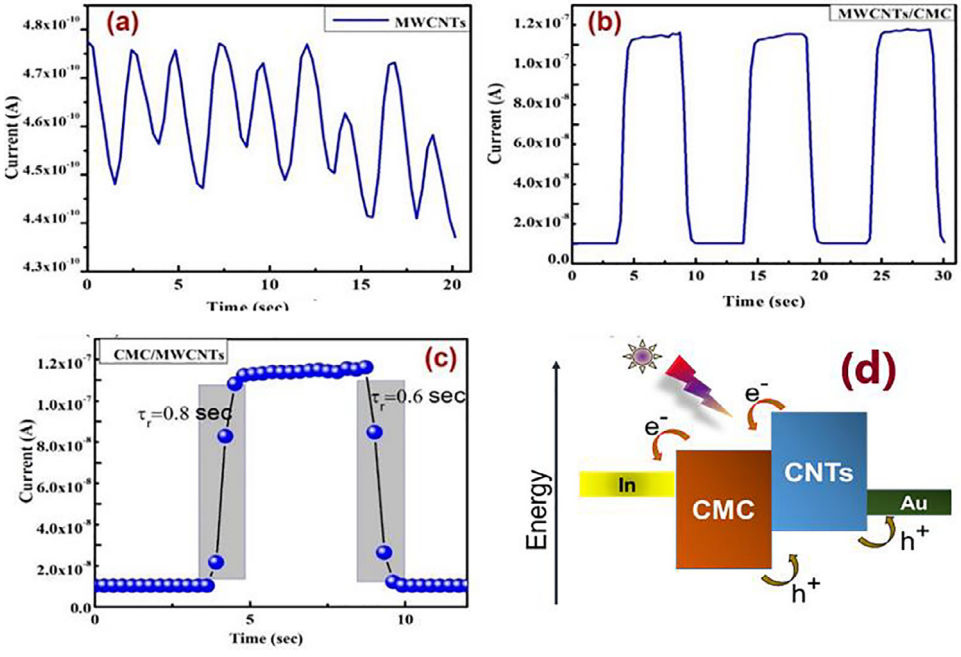

Fig. 6. Photo response characteristics of N- MWCNTs and N-MWCNTs - Na-CMC polymer composite.

Table 9
Values of the enthalpic acid base constants K_A and K_D (unitless) and the entropic acid base constants ω_A and ω_D (unitless) of N-MWCNT (a), Na-CMC (b) and MWCNT-Na-CMC (c) surfaces and their acid base ratios for the different used molecular models and IGC methods.

N-MWCNT (a) Models and IGC methods	K_A	K_D	K_D/K_A	$10^3.\omega_A$	$10^3.\omega_D$	ω_D/ω_A
Kiselev	0.85	1.44	1.69	2.2	4.4	2.0
Spherical	0.71	1.49	2.11	1.9	4.6	2.5
Geometric	0.89	1.02	1.16	2.3	3.2	1.4
Van der Waals	0.70	1.64	2.35	1.8	4.8	2.6
Redlich-Kwong	0.99	1.63	1.65	1.8	4.8	2.6
Cylindrical	0.99	0.77	0.78	2.5	2.7	1.1
Hamieh model	0.89	1.85	2.07	2.1	5	2.3
Topological index	0.72	1.44	2.00	1.9	4.3	2.2
Deformation polarizability	0.55	2.30	4.14	1.6	6	3.8
Vapor pressure	0.74	1.44	1.95	1.9	4.1	2.1
Boiling point *BP*	0.80	1.99	2.49	2.1	5.4	2.6
ΔH^0_{vap}	0.84	2.26	2.69	2.2	5.9	2.7
$\Delta H^0_{vap}(T)$	0.80	2.11	2.63	2	5.7	2.8
Enthalpy of formation ΔH^0_f	0.97	3.69	3.82	2.4	8.9	3.6
Global average	0.82	1.79	2.19	2.1	5	2.4

Na-CMC (b) Models and IGC methods	K_A	K_D	K_D/K_A	$10^4.\omega_A$	$10^3.\omega_D$	ω_D/ω_A
Kiselev	0.03	1.28	44.35	0.15	1.78	117.11
Spherical	0.06	0.82	14.91	0.98	1.14	11.69
Geometric	0.06	0.25	4.41	1.55	0.15	0.97
Van der Waals	0.06	0.63	11.51	1.29	0.91	7.06
Redlich-Kwong	0.04	0.47	11.27	1.18	0.60	5.08
Cylindrical	0.06	0.43	7.62	2.19	0.11	0.50
Hamieh model	0.09	0.17	2.00	1.25	0.85	6.8
Topological index	0.05	0.90	20.00	0.82	1.90	23.17
Deformation polarizability	0.19	0.12	0.65	2.75	0.28	1.02
Vapor pressure	0.03	0.50	16.50	0.61	0.75	12.25
Boiling point *BP*	0.02	0.34	20.85	0.35	0.56	15.85
ΔH^0_{vap}	0.02	0.14	9.33	0.25	0.28	11.11
$\Delta H^0_{vap}(T)$	0.02	0.16	6.54	0.84	0.29	3.45
Enthalpy of formation ΔH^0_f	0.01	0.34	29.97	0.22	2.57	116.68
Global average	0.05	0.47	14.28	1.17	0.83	7.06

N-MWCNT-Na-CMC (c) Models and IGC methods	K_A	K_D	K_D/K_A	$10^4.\omega_A$	$10^3.\omega_D$	ω_D/ω_A
Kiselev	0.16	1.33	22.87	1.7	2.8	17.1
Spherical	0.18	1.12	6.23	4.3	2.3	5.2
Geometric	0.22	0.51	2.33	5.8	0.7	1.1
Van der Waals	0.19	1.02	5.29	4.7	2.1	4.6
Redlich-Kwong	0.19	0.88	4.54	4.6	1.7	3.7
Cylindrical	0.23	0.58	2.47	7.4	0.4	0.6
Hamieh model	0.27	0.57	2.10	8.3	1.2	1.5
Topological index	0.18	1.14	6.33	3.8	2.7	6.9
Deformation polarizability	0.31	0.55	1.76	6.6	1.3	1.9
Vapor pressure	0.14	0.85	6.27	3.4	1.8	5.4
Boiling point *BP*	0.11	0.82	7.21	2.7	1.8	6.9
ΔH^0_{vap}	0.09	0.57	6.20	2.2	1.3	5.8
$\Delta H^0_{vap}(T)$	0.14	0.60	4.25	4.1	1.3	3.1
Enthalpy of formation ΔH^0_f	0.11	1.14	10.78	0.2	4.8	246.5
Global average	0.17	0.83	4.81	4.3	1.9	4.4

than 7%):

$$X(N-MWCNTs-Na-CMC) = \sqrt{X(N-MWCNTs)}\,\sqrt{X(BNa-CMC)} \quad (23)$$

X can be one of the following acid base parameters of the materials: K_A, K_D, ω_A and ω_D.

Eq. (23) also show the dependency of N-MWCNTs-Na-CMC polymer composite on its original components, such as Na-CMC and N-MWCNTs.

4.2. UV-photo detectors

Fig. 6 presents the typical current-time photoresponse properties of the prepared samples under the UV light illumination with a power density of 3.23 mW/cm^2 under zero bias. It can be seen that the pristine CNT PD showed almost negligible response to the UV light as shown in the Fig. 6(a). Whereas, the N-MWCNTs-Na-CMC heterostructure (Fig. 6(b)) showed an obvious photocurrent response which was significantly increased and reached a maximum photocurrent value of $\sim 1.12 \times 10^{-7}$ to the incident UV light. The analyses results indicate stable and reproducible photo switching response curves for the three consecutive cycles without any interruption and decay in the response curves. Furthermore, we have estimated the time-correlated photocurrent rising and falling times of the N-MWCNTs-Na-CMC heterostructure PD. In which the rising/falling times "Tr/Tf" was defined as the maximum time taken to reach from 10% to 90% of its final value of photocurrent, and time required to reach from 90% to 10 % of its baseline value, and

the calculated response/recovery times of the N-MWCNTs-Na-CMC heterostructure PD was found as 0.8/0.6 s. Nevertheless, to explore the excellent self-powered UV photodetection properties of the N-MWCNTs-Na-CMC heterostructure PD, we proposed a possible band alignment based on their valence band edges and works functions respectively is depicted in the Fig. 6(d). Upon the absorption of UV light, the N-MWCNTs-Na-CMC heterostructure PD stimulates the generation of electron hole pairs especially in N-MWCNTs-Na-CMC to produce bound excitons and can diffuse via the depletion region between the N-MWCNTs-Na-CMC heterostructure [33,34].

It is to be noted that the N-MWCNTs can act as transparent electrodes that helps to absorb more photons from the UV light and transferred to the Na-CMC conducting polymer, which further leads to generate a large number of charge carriers. Thereby, the photo-induced exciton was effectively separated at the interface junction and then dissociated into the free electrons and holes, moving in the opposite direction to each other towards the Na-CMC and N-MWCNTs, resulting in the enhanced charge carrier's generation that contributes the significant photocurrent properties at zero bias [34,35]. The high photodetection performances of N-MWCNTs-Na-CMC heterostructure PD was attributed to the synergetic coupling effect of the conductive CMC polymer layer to CNTs that effective improves the heterostructure electrical conductivity [16,36]. Moreover, the negligible photo response to the pristine N-MWCNTs was ascribed to its low bandgap value which was fallen in the infrared range, so that the N-MWCNTs device was not able to respond to UV wavelengths. Thus, the photoresponse analyses of the PD suggesting that the developed N-MWCNTs-Na-CMC heterostructure PD has a great potential and practical applicability for the UV light detection.

5. Conclusion

Inverse gas chromatography method has been applied successfully for the surface thermodynamic characterization of N-MWCNTs, Na-CMC and N-MWCNTs-Na-CMC polymer composite in the temperature range 353.15 K–383.15 K. The determination of the retention time of the different solvents adsorbed on the various materials led to the determination of the free energy of adsorption as a function of the temperature and therefore to the evaluation of the London dispersive surface energy, the specific free energy, enthalpy and entropy of adsorption by using 14 IGC methods and molecular models. We proved that the sum of the free energies of adsorption relative to Na-CMC and N- MWCNTs was equal to the free energy of adsorption of N-MWCNTs - Na-CMC. The Lewis acid base parameters were determined for the above three materials. The dispersive component of the surface energy of materials was obtained as a function of the temperature for all models and methods. The more accurate results were obtained by using Hamieh model that took into account the effect of the temperature on the surface area of the organic molecules. The following relations were obtained:

$$\gamma_s^d(T)\ (N-MWCNTs) = -1.16\,T + 481.68$$

$$\gamma_s^d(T)\ (Na-CMC) = -0.44\,T + 184.01$$

$$\gamma_s^d(T)\ (N-MWCNTs-CMC) = -0.71\,T + 294.95$$

A basic character was proved for the three polymeric materials. The highest Lewis acid base character was obtained for N-MWCNTs. The application of Hamieh model led, for N-MWCNTs, to $K_A = 0.89$, $K_D = 1.85$, $\omega_A = 2.1 \times 10^{-3}$ and $\omega_D = 5 \times 10^{-3}$; for N-MWCNTs-Na-CMC, $K_A = 0.27$, $K_A = 0.57$, $\omega_A = 8.3 \times 10^{-4}$ and $\omega_D = 1.2 \times 10^{-3}$; and for Na-CMC, $K_A = 0.09$, $K_D = 0.17$, $\omega_A = 1.25 \times 10^{-4}$ and $\omega_D = 8.5 \times 10^{-4}$. All used models and methods led to the following classification in decreasing order of the acid base constants of materials:

$$(N-MWCNTs) > (N-MWCNTs-Na-CMC) > (Na-CMC)$$

The results proved that the N-MWCNTs surface contains the highest Lewis basic sites and can interact strongly with Lewis acidic media. Overall, IGC provides useful complementary information on the surface changes resulted from the chemical modifications of the surface. The photo detector application study was also applied for both N- MWCNTs and N-MWCNTs - Na-CMC polymer composite, under the UV illumination (382 nm). The hybrid device showed an enhanced photoresponse to the incident UV light with short response/recovery and high response as compared to the pristine counterparts, which due to the improved electrical conductivity and excellent charge transfer between the hybrid heterostructure.

Ethical approval

This article does not contain any studies with human participants or animals performed by any of the authors.

Declaration of Competing Interest

The authors declare that they have no known competing financial interests or personal relationships that could have appeared to influence the work reported in this paper.

CRediT authorship contribution statement

Basivi Praveen Kumar: Conceptualization, Formal analysis, Investigation, Methodology, Validation, Writing – original draft. **Pasupuleti Visweswara Rao:** Conceptualization, Investigation, Validation, Writing – review & editing. **Tayssir Hamieh:** Conceptualization, Formal analysis, Investigation, Methodology, Supervision, Validation, Writing – review & editing. **Chang Woo Kim:** Conceptualization, Formal analysis, Methodology, Supervision, Validation, Writing – review & editing.

Acknowledgments

This research was supported by Basic Science Research Program through the National Research Foundation of Korea (NRF) funded by the Ministry of Education (2020R1I1A3072987).

Supplementary materials

Supplementary material associated with this article can be found, in the online version, at doi:10.1016/j.chroma.2022.462997.

References

[1] M. Yadav, K.Y. Rhee, S.J. Park, Synthesis, and characterization of graphene oxide/carboxymethylcellulose/alginate composite blend films, Carbohyd. Polym. 110 (2014) 18–25.
[2] S. Ebrahimzadeh, B. Ghanbarzadeh, H. Hamishehkar, Physical properties of carboxymethyl cellulose-based nano-biocomposites with Graphene nano–platelets, Int. J. Biol. Macromol. 84 (2016) 16–23.
[3] B. Praveen Kumar, T.V.M. Sreekanth, S. Ramesh, C. Thota, P.V. Rao, Surface characterization and london dispersive surface free energyof functionalized single-walled carbon nanotubes with a blend of polytetrafluoroethyleneby inverse gas chromatography, Surf. Interface Anal. 51 (2019) 516–524.
[4] S. Ramanaiah, B. Praveen Kumar, P. Venkateswarlu, Surface thermodynamics of poly (caprolactone) diol by inverse gas chromatography, Int. J. Polym. Anal. Charact. 20 (2015) 414.
[5] T. Hamieh, F. Al-Ali, A. Ali-Ahmad, K. Chawraba, J. Toufaily, Z. Youssef, N. Tabaja, T. Roques-Carmes, J. Lalevée, New methodology to determine the surface energy, specific interactions and acid-base properties of titanium dioxide by inverse gas chromatography, Int. J. Chem. Sci. 19 (3) (2021) 1–17.

[6] B. Praveen Kumar, P. Visweswara Rao, S. Ramanaiah, T. Madhusudana Reddy, K.S. Reddy, S.J. Park, Inverse gas chromatography study on London dispersive surface free energy and electron acceptor-donor of fluconazole drug, J. Chem. Eng. Data 62 (2017) 2090–2094.

[7] W. Khan, R. Sharma, P. Chaudhury, A. Siddiqui, P. Saini, Synthesis of carboxylic functionalized multi wall carbon nanotubes and their application for static charge dissipative fibers, Int. J. Nanomater. Nanotechnol. Nanomed. 2 (1) (2016) 025–028.

[8] A.M. Khalil, M.L. Hassan, A.A. Ward, Novel nanofibrillated cellulose/polyvinylpyrrolidone/silver nanoparticles films with electrical conductivity properties, Carbohydr. Polym. 157 (2017) 503–511.

[9] A.B. Abou Hammad, M.E. Abd El-Aziz, M.S. Hasanin, S. Kamel, A novel electromagnetic biodegradable nanocomposite based on cellulose, polyaniline, and cobalt ferrite nanoparticles, Carbohydr. Polym. 216 (2019) 54–62, doi:10.1016/j.carbpol.2019.03.038.

[10] S. Ramesh, K. Karuppasamy, H.M. Yadav, J.J. Lee, K.H. Seok, K. Heung-Soo, K. Joo-Hyung, Ni $(OH)_2$-decorated nitrogen doped MWCNT nanosheets as an efficient electrode for high performance supercapacitors, Sci. Rep. 9 (2019) 1–10 6034, doi:10.1038/s41598-019-42281-z.

[11] S. Ramesh, Y. Haldorai, A. Sivasamy, H.S. Kim, Nanostructured Co_3O_4/nitrogen doped carbon nanotube composites for high performance supercapacitors, Mater. Lett. 206 (2017) 39–43.

[12] S. Ramesh, D. Vikraman, H.S. Kim, H.S. Kim, J.H Kim, Electrochemical performance of MWCNT/GO/$NiCo_2O_4$ decorated hybrid nanocomposite for supercapacitor electrode materials, J. Alloy. Compd. 765 (2018) 369–379.

[13] S. Vijayakumar, G. Muralidharan, Electrochemical supercapacitor behavior of α-Ni $(OH)_2$ nanoparticles synthesized via green chemistry route, J. Electroanal. Chem. 727 (2014) 53–58.

[14] S. Ramesh, A. Kathalingam, K. Karuppasamy, H.S. Kim, H.S Kim, Nanostructured CuO/Co_2O_4@ nitrogen doped MWCNT hybrid composite electrode for high-performance supercapacitors, Compos. Part B Eng. 166 (2019) 74–85.

[15] V. Kakani, S. Ramesh, H.M. Yadav, K. Ashok Kumar, S. Shinde, S. Sandhu, L.N.D. Quang, S. Kim Heung, H.S. Kim, H. Kim, C. Bathula, Facile synthesis of CuO/NiO/nitrogen doped rGO by ultrasonication for high performance supercapacitors, J. Alloy. Compd. 847 (2020) 156411.

[16] K. Ashok, M.A. Khan, M. Kumar, Recent advances in 2D materials-based UV photodetectors: a review, J. Phys. D Appl. Phys. 55 (2021) 1–50 133002, doi:10.1088/1361-6463/ac33d7.

[17] D. Vikraman, I. Rabani, S. Hussain, K. Sundaram, S. Ramesh, K. Heung-Soo, Y.S. Seo, J. Jung, H.S. Kim, Mixed-phase MoS_2 decorated reduced graphene oxide hybrid composites for efficient symmetric supercapacitors, Int. J. Energy Res. 45 (2021) 9193–9209.

[18] H.M. Yadav, S. Ramesh, K. Ashok, S. Shinde, S. Sandhu, A. Sivasamy, N.K. Shrestha, K.H. Soo, K. Hyun-Seok, C. Bathula, Impact of polypyrrole incorporation on nickel oxide@multi walled carbon nanotube composite for application in supercapacitors, Polym. Test. 89 (2020) 106727.

[19] S. Ramesh, D. Vikraman, K. Karuppasamy, H.M. Yadav, S. Arumugam, K. Hyun-Seok, K. Joo-Hyung, K. Heung-Soo, Controlled synthesis of SnO_2@$NiCo_2O_4$/nitrogen doped multiwalled carbon nanotube hybrids as an active electrode material for supercapacitors, J. Alloy. Compd. 794 (2019) 186–194.

[20] Q. Tang, Y. Zhou, L. Ma, M. Gan, Hemispherical flower-like N-doped porous carbon/$NiCo_2O_4$ hybrid electrode for supercapacitors, J. Solid State Chem. 269 (2019) 175–183.

[21] H. Jiang, J. Ma, C. Li, Hierarchical porous $NiCo_2O_4$ nanowires for high-rate supercapacitors, Chem. Commun. 48 (2012) 4465–4467.

[22] J.R. Conder, J.H. Purnell, Gas chromatography at finite concentrations. Part 2.—a generalized retention theory, Trans. Faraday Soc. 64 (1968) 3100–3111.

[23] J.R. Conder, J.H. Purnell, Gas chromatography at finite concentrations. Part 3.—theory of frontal and elution techniques of thermodynamic measurement, Trans. Faraday 65 (1969) 824–838, doi:10.1039/TF9696500824.

[24] J.R. Conder, C.L. Young, Physical Measurements by Gas Chromatography, Wiley J and Sons, New York, 1979.

[25] B. Praveen Kumar, S. Ramanaiah, T. Madhusudana Reddy, K.S. Reddy, Surface characterization of cellulose acetate propionate by inverse gas chromatography, Polym. Bull. 71 (2014) 125–132.

[26] B. Praveen Kumar, S. Ramanaiah, T. Madhusudana Reddy, K.S. Reddy, Surface thermodynamics of efavirenz and a blend of efavirenz with cellulose acetate propionate by inverse gas chromatography, Surf. Interface Anal. 48 (2016) 4–9.

[27] T. Hamieh, J. Schultz, Etude par chromatographie gazeuse inverse de l'influence de la température sur l'aire de molécules adsorbées, J. Chim. Phys. 93 (1996) 1292–1331.

[28] T. Hamieh, Study of the temperature effect on the surface area of model organic molecules, the dispersive surface energy and the surface properties of solids by inverse gas chromatography, J. Chromatogr. A 1627 (2020) 461372.

[29] T. Hamieh, J. Schultz, New approach to characterize physicochemical properties of solid substrates by inverse gas chromatography at infinite dilution, J. Chromatogr. A 969 (1-2) (2002) 17–47, doi:10.1016/S0021-9673(02)00368-0.

[30] T. Hamieh, M. Rezzaki, J. Schultz, Study of the transition temperatures and acid-base properties of poly (methyl methacrylate) adsorbed on alumina and silica, by using inverse gas chromatography technique, Colloids Surf. A 189 (1-3) (2001) 279–291, doi:10.1016/S0927-7757(01)00597-0.

[31] T. Hamieh, Determination of the transition phenomena of Poly(α-n-alkyl) methacrylates adsorbed on silica by inverse gas chromatography (IGC), J. Polym. Res. 18 (2011) 1159–1168, doi:10.1007/s10965-010-9519-9.

[32] M.M. Chehimi, M.L. Abel, C. Perruchot, M. Delamar, S.F. Lascelles, S.P. Armes, The determination of the surface energy of conducting polymers by inverse gas chromatography at infinite dilution, Synth. Met. 104 (1999) 51–59.

[33] Z. Wang, R. Zheng, Na Wang, H. San, Self-driven photoelectrochemical UV-visible photodetectors using ZrO_2@ TiO_2 core-shell nanorod arrays modified with single-walled carbon nanotubes, in: Proceedings of the IEEE 16th International Conference on Nano/Micro Engineered and Molecular Systems (NEMS), IEEE, 2021.

[34] K.S. Pasupuleti, M. Reddeppa, B.G. Park, J.E. Oh, S.G. Kim, M.D. Kim, Efficient charge separation in polypyrrole/gan-nanorod-based hybrid heterojunctions for high-performance self-powered UV photodetection, Phys. Status Solidi (RRL) Rapid Res. Lett. 15 (12) (2021) 1–6 2000518. In this issue, doi:10.1002/pssr.202000518.

[35] V.H. Vuong, S.V.N. Pammi, K.S. Pasupuleti, W. Hu, J.S. Van Dang Tran, M.D. Kim, V. Pecunia, Soon gil yoon, engineering chemical vapor deposition for lead-free perovskite-inspired MA3Bi2I9 self-powered photodetectors with high performance and stability, Adv. Opt. Mater. 9 (12) (2021) 1–10 2100192, doi:10.1002/adom.202100192.

[36] Y.T. Li, K. Sun, Di Luo, Y.M. Wang, L. Han, H. Liu, X.L. Guo, D.L. Yu, T.L. Ren, A review on low-dimensional novel optoelectronic devices based on carbon nanotubes, AIP Adv. 11 (11) (2021) 110701.

[37] C. Kemball, E.K. Rideal, The adsorption of vapours on mercury I) Non –polar substances, Proceedings of the Royal Society of London. Series A 187 (1946) 53–73.

[38] C. Saint Flour, E. Papirer, Gas-solid chromatography. A method of measuring surface free energy characteristics of short glass fibers. 1. Through adsorption isotherms, Ind. Eng. Chem. Prod. Res. Dev. 21 (1982) 337–341, doi:10.1021/i300006a029.

[39] C. Saint Flour, E. Papirer, Gas-solid chromatography: method of measuring surface free energy characteristics of short fibers. 2. Through retention volumes measured near zero surface coverage, Ind. Eng. Chem. Prod. Res. Dev. 21 (1982) 666–669, doi:10.1021/i300008a031.

[40] D.T. Sawyer, D.J. Brookman, Anal. Chem. 40 (1968) 1847–1850.

[41] J.B. Donnet, S. Park, H. Balard, Evaluation of specific interactions of solid surfaces by inverse gas chromatography, Chromatographia 31 (1991) 434–440.

[42] E. Brendlé, E. Papirer, A new topological inde T for molecular probes used in inverse gas chromatography for the surface nanorugosity evaluation, 1. Method of evaluation, J. Colloid Interface Sci. 194 (1997) 207–216.

[43] E. Brendlé, E. Papirer, H. Balard, J. Dentzer, Variation of the surface properties of nickel o tide upon heat treatment evidenced by temperature programmed desorption and inverse gas chromatography studies, J. Mater. Sci. 35 (2000) 3573–3577.

[44] H. Balard, M. Sidqi, E. Papirer, J.B. Donnet, A. Tuel, H. Hommel, A.P. Legarnd, Study of modified silicas by inverse gas chromatography part II: influence of chain length on surface properties of silicas grafted with α–ω diols, Chromatographia 25 (1988) 712–716.

[45] I, 337-372 F.M. Fowkes, J.D. Andrade, Surface and Interfacial Aspects of Biomedical Polymers Plenum Press, New York, 1985. I, 337-372.

[46] G.M. Dorris, D.G. Gray, Adsorption of normal-alkanes at zero surface coverage on cellulose paper and wood fibers, J. Colloid Interface Sci. 77 (1980) 353–362.

[47] T. Hamieh, A.A. Ahmad, T. Roques-Carmes, J. Toufaily, New approach to determine the surface and interface thermodynamic properties of H-β-zeolite/rhodium catalysts by inverse gas chromatography at infinite dilution, Sci. Rep. 10 (1) (2020) 1–27.

[48] T. Hamieh, New methodology to study the dispersive component of the surface energy and acid-base properties of silica particles by inverse gas chromatography at infinite dilution, J. Chromatogr. Sci. (2021) bmab066, doi:10.1093/chromsci/bmab066.

[49] T. Hamieh, A.A. Ahmad, A. Jrad, T. Roques-Carmes, M. Hmadeh, J. Toufaily, Surface thermodynamics and Lewis acid-base properties of metal-organic framework crystals by inverse gas chromatography at infinite dilution, J. Chromatogr. A 1666 (2022) 462849.

[50] T.V.M. Sreekanth, B. Praveen Kumar, P.C. Nagajyothi, G.R. Dillip, T.J. Shim, K.K. Yoo, Determination of surface properties and Gutmann's Lewis acidity–basicity parameters of thiourea and melamine polymerized graphitic carbon nitride sheets by inverse gas chromatography, J. Chromatogr. A 1580 (2018) 134–141.

[51] A. Kondor, C. Quellet, D. Dallos, Surface characterization of standard cotton fibres and determination of adsorption isotherms of fragrances by IGC: surface characterization of cotton and adsorption of fragrances by IGC, Surf. Interface Anal. 47 (2015) 1040–1050.

[52] B. Praveen Kumar, P. Visweswara Rao, T. Hamieh, Surface thermodynamic properties of sodium carboxymethyl cellulose by inverse gas chromatography, Chem. Eng. J. Adv. 9 (2022) 100207.

[53] P.K. Basivi, S. Ramesh, V. Kakani, et al., Ultrasonication-mediated nitrogen-doped multiwalled carbon nanotubes involving carboxy methylcellulose composite for solid-state supercapacitor applications, Sci. Rep. 11 (2021) 9918, doi:10.1038/s41598-021-89430-x.